Flow Turbulence Combust (2009) 82:455–475
DOI 10.1007/s10494-008-9183-x

Second-Order Conditional Moment Closure Simulations of Autoignition of an n-heptane Plume in a Turbulent Coflow of Heated Air

G. De Paola · I. S. Kim · E. Mastorakos

Received: 7 January 2008 / Accepted: 15 October 2008 / Published online: 5 December 2008

Abstract Autoignition of an n-heptane plume in a turbulent coflow of heated air has been studied using the conditional moment closure (CMC) method with a second-order closure for the conditional chemical source term. Two different methodologies have been considered: (i) the Taylor expansion method, in which the second order correction was based on the solution of the full covariance matrix for the 31 reactive species in the chemical mechanism and hence was not limited to a few selected reactions, and (ii) the conditional PDF method, in which only the temperature conditional variance equation has been solved and its PDF assumed to be a β-function. The results compare favorably with experiment in terms of autoignition location. The structure of the reaction zone in mixture fraction space has been explored. The relative performance of the two methodologies is discussed.

Keywords Turbulent autoignition · Second-order CMC

1 Introduction

Autoignition of turbulent inhomogeneous mixtures is a problem of fundamental importance and practical interest. The development of combustion devices such as Homogeneous Charge Compression Ignition (HCCI) engines and Lean Premixed Pre-vaporized (LPP) gas turbines, in terms of improved efficiency and reduced emissions, can be significantly aided by a better understanding and ability to predict

G. De Paola (✉) · I. S. Kim · E. Mastorakos
Hopkinson Laboratory, Department of Engineering,
University of Cambridge, Cambridge, CB2 1PZ, UK
e-mail: gd257@cam.ac.uk

I. S. Kim
e-mail: isk20@cam.ac.uk

E. Mastorakos
e-mail: em257@eng.cam.ac.uk

the phenomenon of autoignition. At autoignition, the fluid mechanics and chemical timescales are of the same order of magnitude and a combustion model able to adequately resolve the coupling between turbulence and chemistry is necessary.

Using a two-dimensional DNS with a mixing layer configuration between hot air and cold fuel and chemistry represented by an irreversible one-step reaction, Mastorakos et al. [1] analyzed the autoignition event in terms of local reactant concentrations as function of the conserved scalar mixture fraction (ξ) and the scalar dissipation rate ($\chi = 2D(\nabla\xi)^2$). It was shown that inhomogeneous mixtures autoignite at a well-defined mixture composition defined as the 'most-reactive' ξ_{MR}, dependent on the reaction kinetics, the initial composition, the initial temperature of the reactants and the scalar dissipation rate. Among the different possible autoignition locations the one with lowest scalar dissipation rate $\chi|\xi_{MR}$ ignites first due to smaller heat losses due to the lower scalar gradients. The effect of turbulence was also investigated. It was concluded that increasing the velocity fluctuations u' will shorten the autoignition delay τ_{IGN}. This was explained as an indirect effect that turbulence has on the mixing field, rather than as a direct relation between the turbulent timescale τ_{TURB} and τ_{IGN}. High initial value of u' enhances the appearance of ξ_{MR} and eventually creates well-mixed spots with reduced gradient ($\chi|\xi_{MR}$), with the overall effect of increasing the probability of autoignition. These conclusions were extended in later work by Im et al. [2], Sreedhara and Lakshmisha [3] and Echekki and Chen [4] using more realistic chemistry and a three-dimensional flow field. More recently Wang and Rutland [5] performed DNS of an autoigniting spray jet. The work underlined that in presence of an evaporating droplets, their size and momentum have an effect on autoignition through the effect of distribution in the turbulent field and cooling.

Modelling work was carried by Mastorakos et al. [6] to evaluate the effect of mixing on autoignition. The results for laminar autoignition from Liñan and Crespo [7] and Thevenin and Candel [8] were extended to turbulent flows. Autoignition is inhibited by high value of $\chi|\xi_{MR}$. A critical value can be observed, χ_{CR}, so that for $\chi|\xi_{MR} > \chi_{CR}$ autoignition can not occur. In a turbulent flow the fluctuations of scalar dissipation rate above its conditional mean can be significant, $\chi''|\xi_{MR}$, hence even if its average value $\langle\chi|\xi_{MR}\rangle$ is above χ_{CR}, instantaneously reaction can proceed leading to ignition. These studies suggest that a conserved scalar approach has to be preferred in order to explicitly account for the effect of ξ_{MR} and $\chi|\xi_{MR}$. The Conditional Moment Closure [9] has been, therefore, selected among the different models due to its general mathematical formulation, which does not imply any assumptions on the topology of the reaction zone.

DNS plots of conditional temperature during the thermal 'run-away' at ignition show large scatter, highlighting that the common assumption of negligible conditional fluctuations necessary for a first-order CMC closure may be too restrictive. A more complete formulation based on higher-order closure for the reaction rate or double conditioning can be necessary when the effects of conditional fluctuations are significant. Mastorakos and Bilger [10] compared the results of CMC using first and second-order closure with the prediction of autoigniting DNS. The reaction rate was calculated based on a one-step irreversible reaction and a Taylor expansion series truncated at second-order was used to approximate the exponential in the conditional chemical source term in the second-order closure. The second-order

correction needed the conditional temperature variance, for which an equation was solved. DNS and second-order predictions compared favorably. It was also shown that CMC predictions with first and second-order closure were similar at low $\langle \chi | \eta \rangle$, while they diverged for higher values and, in particular for $\langle \chi | \eta \rangle > \chi_{CR}$, first-order closure failed to predict ignition. At this latter condition, the process is driven by the fluctuations of the conditional scalar dissipation rate so that second-order closure is necessary.

Sreedhara and Lakshmisha [11] revisited the above analysis using a 3D DNS database of autoignition and a reaction mechanism with four reactions. The use of a more complex chemistry introduced the effect of the scalar conditional covariances in the autoignition prediction. It was shown that for complex chemistry the modelling of species and temperature covariances is also important; the influence of the species conditional fluctuations was included as a correction term and a selection of the most critical species and reactions was advanced. In both cases presented, the model was able to predict the autoignition time, but the linear approximation of the exponential in the reaction rate, due to the Taylor series expansion, could not proceed after autoignition.

CMC modelling for autoignition is yet limited either to higher-order closure with very simple chemical kinetics [10, 11] or to more complex mechanism using a first-order closure [12]. To the authors' knowledge, a study on the limit of applicability of first and second-order closure to model turbulent autoignition with detailed chemistry has not been done before. Furthermore, a numerical methodology able to predict the influence of conditional fluctuations on autoignition and its transition to the subsequent flame kernel development can prove useful to model the 'premix' phase of diesel engine combustion as well as HCCI combustion.

Additional work worth mentioning is the application of second-order CMC in the context of flames with localized extinction/reignition [13–15]. Sreedhara and Huh [14] applied the second order correction to three rate-limiting chemical steps to avoid solving the entire set of conditional covariance whereas Fairweather and Woolley [15] identified a two-step global reaction mechanism and applied the second order correction based on two progress variables. In both cases a Taylor expansion method for the conditional reaction rate closure was considered. Both papers showed improvement in the prediction of major and minor species with respect to a first-order closure.

The calculations presented in this paper focus on the experiment by Markides and Mastorakos [16, 17], described in the next section. This experiment has been selected as one of a few experiments where mixing effects on autoignition have been directly explored and some sensitivity has been shown. Numerical modelling of the present autoignition experiment using a first-order CMC model [12] has demonstrated that an increased flow bulk velocity has a delaying effect on autoignition due to the increased mean conditional scalar dissipation rate. The effect of the flow inhomogeneities was also considered demonstrating the effects of the mixture fraction probability density function on autoignition. This experiment has also been modelled with LES [18, 19]. In this paper, limiting the study to relatively high reactant initial temperature in order to have autoignition appearing close to the nozzle and hence in regions of high mixture fraction probability to better isolate the effects of turbulent mixing, a second-order conditional moment closure has been implemented

to evaluate the effects of conditional fluctuations. Given the good prediction of first-order closure in this particular flow configuration the application of second-order closure is not expected to give substantial difference in the autoignition delay results. However, it is implemented here with the particular intent of better analyzing the autoignition phenomenon through the analysis of the conditional second-moments and to validate the numerical methodology, which is still not fully validated in case of turbulent non-premixed autoignition.

In the following, the experimental configuration is outlined. The unclosed conditional transport equation for first and second order closure together with the methods used for its numerical solution are presented in Section 3. Details of previous second-order CMC approaches for flames are included. The results are presented and discussed in Section 4.

2 Experimental Configuration

Details on the configuration and the measurements can be found in Refs. [12, 16] and briefly summarized in this Section. The experiment consisted of an axi-symmetric injection of gaseous fuel into a stream of electrically pre-heated air coflowing in a pipe (Fig. 1). The turbulence was boosted above the usual pipe flow turbulence levels by a grid upstream of the fuel nozzle. To reduce heat losses, the pipe was confined into a vacuum-insulated quartz tube that allowed full optical access. Autoignition, under certain conditions, occurred at a location depending on the fuel (i.e. type, dilution), the initial temperature and the flow velocity. For a certain range of T_{AIR}, U_{AIR} and U_{FU}, individual autoignition events manifested in the form of localized 'flashes'. Each event was associated with an ignition kernel that ignited successfully, propagated and extinguished. Autoignition behavior was statistically steady. Random autoignition events occurred continuously at a well defined mean frequency and location. This regime was define as 'Random Spots' [16]. It was identified as an intermediate and well-defined regime between a 'no ignition' and

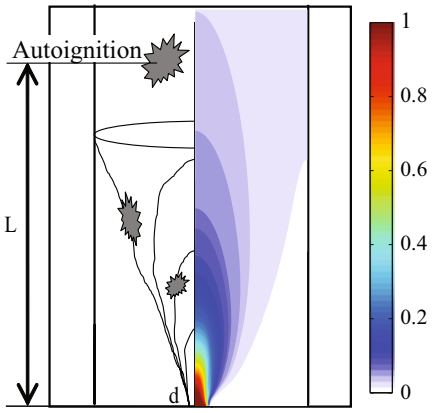

Fig. 1 *Left*: experimental apparatus (reproduced from [12]), with schematic of mixture fraction isolines. Fuel injection at the centre. *Right*: isocontours of calculated mean mixture fraction $\widetilde{\xi}$

an intermediate pre-ignition regime in which no proper autoignition took place; and the 'flash-back regime' in which the autoignition spot instead of quenching gave rise to an attached or lifted flame.

Autoignition was detected by chemiluminescence from the hydroxyl radical (OH^*) collected by an intensified camera. The autoignition length (L_{IGN}) was hence determined as the axial distance from the injector to the autoigniting region. Two definitions were used: L_{MIN} corresponding to the axial location of a 3% rise in the average signal intensity, with the average performed over many realizations, and L_{MODE} corresponding to the axial location of the maximum average OH^* signal. For the set of experiments considered in this paper, the air was at T_{AIR} of 1100–1140 K. Pre-vaporized nitrogen-diluted n-heptane (C_7H_{16}) was used as fuel, with the mass fraction of C_7H_{16} kept constant at $Y_{C_7H_{16}} = 0.95$. The non-dimensional velocity ratio $\upsilon = U_{FUEL}/U_{AIR}$ ranged between 1.05 and 1.20. The fuel stream was injected at temperatures (T_{FUEL}) in the range 1020–1050 K, with the difference between T_{FUEL} and T_{AIR} within 70–100 K.

2.1 Formulation

2.2 CFD

As the heat release before autoignition is very small, the density changes prior to autoignition can be neglected, allowing the assumption of frozen mixing and the decoupling between the CFD and the CMC solver. The velocity and mixture fraction fields were predicted by the solution of an axi-symmetric problem using the commercial CFD software FLUENT [20]. The CFD mesh, highly refined along the axis and close to the injector exit with a radial size at the injector exit of $d/20$, extended for the full length of the quartz-tube and incorporated a total of 64500 cells giving a grid independent solution. The flow field was computed using a Reynolds stress turbulence model (RSM). The mixing field has been calculated solving transport equations for mixture fraction ($\widetilde{\xi}$) and mixture fraction variance ($\widetilde{\xi''^2}$). Additional transport equations have been solved for the scalar flux ($\widetilde{\mathbf{v}''\xi''}$) and the mean scalar dissipation ($\widetilde{\chi}$) rate following the implementation reported by Kim and Mastorakos [21], which should be consulted for details. The use of these extra transport equations is motivated by the need to capture well the early mixing region close to the injector. In this region, the rapid decay of the scalar dissipation rate was not adequately captured with a simple algebraic closure because the usual model based on a constant timescale ratio between the scalar and velocity fluctuations is not accurate in the early stages of mixing [17]. Boundary conditions based on the measured turbulent intensity and length scale at the nozzle plane were imposed at the inlet. At the wall, zero gradient boundary conditions were used for the mean and variance mixture fraction and the unconditional scalar dissipation, while zero values were used for the mixture fraction turbulent flux. Outflow boundary conditions were used for the downstream exit. Table 1 summarizes the conditions used in the calculations. It is important to stress that the decoupling between the CFD and the CMC calculation is possible only under the hypothesis of small heat release, which holds until autoignition. At high temperature the dilatation due to the density effects affects the flame expansion. The results that will be presented in the next section

Table 1 Conditions investigated for the separate velocity, mixing, and autoignition measurements

Type	U_{AIR} $[m/s]$	υ $[-]$	T_{AIR} $[K]$	T_{FU} $[K]$	ρ_{AIR} $[kg/m^3]$	ρ_{FU} $[kg/m^3]$
Velocity	2.66	1.08	297	297	1.180	1.180
Mixing	3.09	1.17	473	438	0.747	0.919
Autoignition	17.64	1.20	1100–1140	1020–1050	0.313	1.030

$\upsilon = U_{FU}/U_{AIR}$

describing the flame propagation after autoignition are important only in the context of a qualitative description of the phenomenon and as a validation of the numerical method, rather than as a quantitative prediction of the rate of expansion.

2.3 CMC

First and second-order CMC [9] has been applied, denoted respectively as CMCI and CMCII. Conditional means and covariances can be defined respectively as $Q_i = \langle Y_i|\eta\rangle$, $G_{ij} = \langle Y_i'' Y_j''|\eta\rangle$, where the double prime represents the fluctuation above the conditional mean.

The flow field and the phenomena analyzed have been considered as parabolic. A space-marching formulation has been applied, hence neglecting the effect of axial diffusion. This assumption means that the simulations cannot capture the flashback regime observed in the experiment under some conditions, and hence emphasis is placed only on experimental conditions where no continuous flame was stabilised. Under the hypothesis of thin boundary-layer flows, furthermore, it is assumed that the conditional statistics vary little along the cross-stream direction [22] so that the system of equations to solve could be reduced to:

$$\langle v_Z|\eta\rangle^* \frac{\partial Q_i}{\partial z} = \langle N|\eta\rangle^* \frac{\partial^2 Q_i}{\partial \eta^2} + \langle W_i|\eta\rangle \tag{1}$$

$$\begin{aligned}
\langle v_Z|\eta\rangle^* \frac{\partial G_{ij}}{\partial z} = {} & \langle N|\eta\rangle^* \frac{\partial^2 G_{ij}}{\partial \eta^2} && (T_1)\\
& + \langle W_i'' Y_j'' + W_j'' Y_i''|\eta\rangle && (T_2)\\
& - 2\langle D(\nabla Y_i'' \cdot \nabla Y_j'')|\eta\rangle && (T_3)\\
& + \langle Y_j'' N''|\eta\rangle \frac{\partial^2 Q_i}{\partial \eta^2} + \langle Y_i'' N''|\eta\rangle \frac{\partial^2 Q_j}{\partial \eta^2} && (T_4)\\
& + \frac{1}{\rho_\eta P(\eta)} \frac{\partial J_{G_{ij}}}{\partial \eta} && (T_5)\\
& - \langle Y_j'' v_Z''|\eta\rangle \frac{\partial Q_i}{\partial z} - \langle Y_i'' v_Z''|\eta\rangle \frac{\partial Q_j}{\partial z} && (T_6)
\end{aligned} \tag{2}$$

The temperature and the temperature-species covariance equations could be written analogously, under the assumption of adiabatic wall, constant pressure, no heat loss of radiation and low Mach number flow as

$$\begin{aligned}\langle v_Z|\eta\rangle^* \frac{\partial Q_T}{\partial z} &= \langle N|\eta\rangle^* \frac{\partial^2 Q_T}{\partial \eta^2} - \frac{1}{c_{p_\eta}} \left\langle \sum_{i=1}^{n} h_i W_i \middle| \eta \right\rangle \\ &\quad + \langle N|\eta\rangle^* \frac{1}{c_{p_\eta}} \left(\frac{\partial c_{p_\eta}}{\partial \eta} + \sum_{i=1}^{n} c_{p,i_\eta} \frac{\partial Q_i}{\partial \eta} \right) \frac{\partial Q_T}{\partial \eta} \end{aligned} \tag{3}$$

$$\begin{aligned}\langle v_Z|\eta\rangle^* \frac{\partial G_{iT}}{\partial z} &= \langle N|\eta\rangle^* \frac{\partial^2 G_{iT}}{\partial \eta^2} \\ &\quad + \langle W_i'' T'' + (W_T'' Y_i''/c_{p_\eta})|\eta\rangle - 2\langle D(\nabla Y_i'' \cdot \nabla T'')|\eta\rangle \\ &\quad + \left[\langle T'' N''|\eta\rangle \frac{\partial^2 Q_i}{\partial \eta^2} + \langle Y_i'' N''|\eta\rangle \frac{\partial^2 Q_T}{\partial \eta^2} \right. \\ &\quad \left. - \langle Y_i'' N''|\eta\rangle \frac{1}{c_{p_\eta}} \left(\frac{\partial c_{p_\eta}}{\partial \eta} + \sum_{i=1}^{n} c_{p,i_\eta} \frac{\partial Q_i}{\partial \eta} \right) \frac{\partial Q_T}{\partial \eta} \right] \\ &\quad + \frac{1}{\rho_\eta P(\eta)} \frac{\partial J_{G_{iT}}}{\partial \eta} - \langle T'' v_z''|\eta\rangle \frac{\partial Q_i}{\partial z} - \langle Y_i'' v_z''|\eta\rangle \frac{\partial Q_T}{\partial z} \end{aligned} \tag{4}$$

The terms on the right-hand side of (2) have been denoted as T_i to facilitate later discussion. Equations (3) and (4) assume a variable specific heat capacity with temperature so that additional terms appear with respect to the species equations. Derivation of (4) is reported by De Paola [23]. The last term on the right-hand side (T_6) in (2) and (4) has been retained even if on a dimensional analysis its magnitude is comparable to the spatial diffusion term that has been neglected under the hypothesis of parabolic flow. This source term does not directly depend on the G_{ij} and can be estimated from (1) and (3); its magnitude will be assessed in the Results section.

$\langle\cdot|\eta\rangle^*$ is a cross-stream averaging operator defined for the generic variable ψ as

$$\langle \psi|\eta\rangle^* = \frac{\int_0^R \langle \psi|\eta\rangle \bar{\rho} \tilde{P}(\eta) 2\pi r dr}{\int_0^R \bar{\rho} \tilde{P}(\eta) 2\pi r dr} \tag{5}$$

where R is the inner radius of the quartz tube. $\langle\psi|\eta\rangle$ and $\tilde{P}(\eta)$ are evaluated locally in the CFD cells. $\tilde{P}(\eta)$ is the probability density function of the mixture fraction and it is assumed to be a β-function.

The use of the cross stream average formulation is not expected to play a significant role in the prediction of the autoignition length. Experimental measurements have shown that the conditional scalar dissipation rate varies little along the spanwise direction [24]. Furthermore, the use of an averaging weighted by the $\tilde{P}(\eta)$ inherently takes into account the conserved scalar fluctuations. The cross-stream average operator is however limited in the inner region of the quartz tube where autoignition is expected. A more complete elliptic formulation considering the radial direction should be used if the effect of the wall needs to be considered.

A threshold $\tilde{P}(\eta) > 1 \times 10^{-50}$ has been considered to define the region of finite $\tilde{P}(\eta)$ so that the CMC equations are solved within the interval $[\eta_{MIN}, \eta_{MAX}]$,

consistent with the similar choice made by Devaud and Bray [25]. The value of this threshold has been defined so that autoignition occurs within the mixture fraction domain with finite probability with no influence from the region of low probability. Boundary conditions in η-space are set according to Ref. [9]. The $\tilde{P}(\eta)$ evolves from a double δ-function when the reactants are initially segregated at the injector to a single δ at end of the tube. The η-domain of finite $\tilde{P}(\eta)$ always shrinks so no reinitialization is needed for the mixture fractions with zero probability.

Standard modelling approaches have been used to close the unclosed terms: the linear model was used for the conditional velocity ($\langle u_Z|\eta\rangle$) and the Amplitude Mapping Closure (AMC) model for the conditional scalar dissipation rate ($\langle N|\eta\rangle$).

The chemical source term was calculated using a 31 species reduced mechanism for n-heptane [26], which is based on a detailed mechanism with 59 species and 203 reactions due to Hewson [27] and validated elsewhere [12, 28].

The conditional reaction rate has been closed at first-order (CMCI) using (6):

$$\langle W(\mathbf{Y})|\eta\rangle = W(\mathbf{Q}) \tag{6}$$

Two methodologies have been considered for the higher-order closure (CMCII): the Taylor expansion and the joint-PDF method. The first is based on (7) [29]

$$\langle W(\mathbf{Y})|\eta\rangle = \underbrace{W(\mathbf{Q})}_{\langle W^I|\eta\rangle} + \underbrace{\frac{1}{2}\left.\frac{\partial^2 W}{\partial Y_i \partial Y_j}\right|_{\mathbf{Y}=\mathbf{Q}} G_{ij}}_{\langle W^{II}|\eta\rangle} \tag{7}$$

in which the first-order term ($\langle W^I|\eta\rangle$) and the second-order correction ($\langle W^{II}|\eta\rangle$) have been highlighted. $\langle W_T^{II}|\eta\rangle$ has been calculated using the Hessian of the reaction rate evaluated numerically. The full set of conditional variances and covariances of the species in the mechanism have been considered for a total of $n \times (n+1)/2$ additional equations, where n is the number of the reactive species in the chemical mechanism and temperature. Analogously, the term T_2 in the covariance equation has been closed with the numerical evaluation of the Jacobian of the conditional reaction rate as

$$\langle W_i'' Y_j''|\eta\rangle = \left.\frac{\partial W_i}{\partial Y_k}\right|_{\mathbf{Y}=\mathbf{Q}} G_{kj} \tag{8}$$

The use of the full set of covariances rather than only of few important reactions as in Ref. [30] results in a more general methodology that includes conditional fluctuations for all phases of non-premixed combustion from autoignition to the diffusion flame. In this context, the use of a limited number of species and reactions should be considered as a particular case. In flame problems, employing second-order correction to certain reactions only has been motivated by the fact that certain species can be put in quasi-steady state and that some reactions can be put in partial equilibrium. However, such reduction techniques are more difficult to implement in autoignition because the chemical manifold has not been developed yet to the same extent. An alternative way would be to select the species for which to apply the second order correction based on the information of their timescales, but this has not been attempted yet.

The second method employs a presumed shape for the conditional joint-PDF of the scalars and temperature ($\tilde{P}(\mathbf{Y}|\eta)$). Because no clear indication is given in the

literature on its shape during autoignition and justified by the strong dependence on temperature of the reaction rate, in the present work the implementation of the joint-PDF method has been limited to the conditional temperature only. The shape of $P(T|\eta)$ during autoignition can be inferred by the plot of reactedness in Mastorakos et al. [1] noticing that $T|\eta$ is a bounded scalar between its value at cold mixing between fuel and oxidizer ($\langle T|\eta\rangle_{MIX}$) and at equilibrium ($\langle T|\eta\rangle_{EQ}$). The latter was calculated using a separate run of the zero-dimensional CMC code at the same initial temperatures but with low scalar dissipation rate. A presumed two-parameter β-function has been used to model $P(T|\eta)$ as a function of the reduced conditional mean and the reduced conditional variance of temperature respectively defined as

$$\widehat{Q}_T = \frac{Q_T - \langle T|\eta\rangle_{MIX}}{\langle T|\eta\rangle_{EQ} - \langle T|\eta\rangle_{MIX}}; \qquad \widehat{G}_{TT} = \frac{G_{TT}}{(\langle T|\eta\rangle_{EQ} - \langle T|\eta\rangle_{MIX})^2} \tag{9}$$

Using this formulation only one extra transport equation for the temperature variance has to be added to CMCI and the closure for the reaction rate terms in (1) and (2) can be rewritten as

$$\langle W(\mathbf{Y}, T)|\eta\rangle \equiv \int_{\langle T|\eta\rangle_{MIX}}^{\langle T|\eta\rangle_{EQ}} W(\mathbf{Q}, T)\, P(T|\eta) dT \tag{10}$$

$$\langle W_T'' T''|\eta\rangle = \int_{\langle T|\eta\rangle_{MIX}}^{\langle T|\eta\rangle_{EQ}} W_T(\mathbf{Q}, T)\, P(T|\eta) dT - \langle W_T|\eta\rangle\, Q_T \tag{11}$$

For clarity reasons, the temperature dependence of the reaction rate in (10) and (11) has been explicitly stated. To simplify the nomenclature the same symbol, T, will be used for temperature and its sample space. From the S-shape curve describing the ignition/exctintion limit in a laminar counterflow configuration [31], the autoignition limit is not exactly defined at the frozen temperature so a normalization based on a higher value may be needed, although this has not been attempted here. The use of a β-function to model $P(T|\eta)$ has already been used in the literature by Cha and Pitsch [13] and Kronenburg and Kostka [32] in the context of flames with extinction/reignition. Useful comments on the shape of the conditional joint-PDF for a DNS of stably burning flames using a two-reaction mechanism is presented by Swaminathan and Bilger [33]. In the present work the validity of this presumed shape has not been questioned, but further studies on the scalar conditional joint-PDF during the autoignition phase using more complex chemistry are necessary. The validity of this simplified methodology seems reasonable even at later times when eventually a flame is formed, similarly to what proposed by [32] where sensible enthalpy variance was identified as the most important source of fluctuations rather than other reactive species.

Equation (2) is the unclosed form of the conditional covariance transport equation. Closures for the first and second moments need to be consistent, therefore same models as for the conditional mean transport equations have been used when possible: the linear model was employed to close the conditional velocity, the AMC to model the conditional scalar dissipation rate. The gradient diffusion approximation has been applied to model the conditional turbulent flux.

The term T_3 in (2) is a dissipative term and has been modelled as [34]

$$\langle D(\nabla Y_i'' \cdot \nabla Y_j'')|\eta\rangle = \sqrt{C_i C_j}\,\frac{G_{ij}}{\tau_Y} \qquad \text{with} \qquad \tau_Y = C_{\tau_Y}\frac{\widetilde{\xi''^2}^{1/2}}{\tilde{\chi}} \tag{12}$$

τ_Y represent a mixing timescale and is here calculated directly from the scalar dissipation of the mixture fraction (since we are solving a transport equation for it), rather than k and ε to allow for the possibility of a disparity between the scalar and velocity timescales. For the constants, the values $C_i = C_j = 1$ and $C_{\tau_Y} = 2$ have been used.

The term T_4 involving scalar dissipation-scalar fluctuations correlations, has been closed as [34]:

$$\begin{aligned} \langle Y_i'' N''|\eta\rangle &= C_{N''Y''}\langle N|\eta\rangle G_{ii}^{1/2} \\ C_{N''Y''} &= R_{N''Y''}F \qquad \text{with} \qquad F = \frac{\langle N''^2|\eta\rangle^{1/2}}{\langle N|\eta\rangle} \end{aligned} \tag{13}$$

Analysis of DNS of autoignition with a one-step chemistry [1] showed that the correlation coefficient between the two fluctuating quantities $R_{N''Y''}$, is a function of η but does not vary much with the Reynolds number. The correlation coefficient between the conditional temperature and conditional scalar dissipation had a sinusoidal-like function.

Reference [11] found similar results using a four-step chemical mechanism for n-heptane and extracted from their DNS database a correlation coefficient following the shape function

$$R_{N''Y''} = C_{ny}\left[-4.2 * (1-\eta)^6 exp(-0.08/\eta)\right] \tag{14}$$

The model predicts a minimum of -1 in the region near stoichiometry and zero-correlation at the rich mixture fractions since the interest was focused on autoignition and the most reactive region was found close to stoichiometry. A similar shape was also presented by [33] for low Damköhler number reactions. The constant $C_{ny} = 0.8$ has been used to resize the shape function to the value found in Ref. [33]. The sign of $R_{N''Y''}$ is positive or negative respectively for products or reactants. The stoichiometric and the most reactive mixture fraction in the test case modelled here are similar to what reported in [11]. The model, used here in an autoignition case, could give a reasonable representation of the physics, but clearly it can not be considered as 'universal' for all species without a proper validation [35]. Further work is therefore needed in this direction.

The coefficient F appearing in (13) was investigated numerically in [33] and experimentally in [24]. In both cases, it was found to increase with the Reynolds number stabilizing to a constant between $F \in [1-1.3]$, relatively constant in η-space. Due to the fact that the value of F is not as well-studied as the corresponding ratio for the unconditional scalar dissipation, here a sensitivity on this parameter has been performed to evaluate the importance of the conditional scalar fluctuations on autoignition.

The term T_5 in (2) has been modelled as [36]

$$J_{G_{ij}} = C_J \rho_\eta P(\eta) \langle N|\eta \rangle \frac{\partial G_{ij}}{\partial \eta} \tag{15}$$

using the suggested value of $C_J = 1$ for the constant.

A comprehensive analysis of the different closure strategies has been reported by Li and Bilger [34] and Swaminathan and Bilger [33] and more recently presented by Sreedhara and Huh [30]. In these references closures for (8), (12) and (13) have been reported based on steady laminar flamelet tabulation with promising results. An extension in the context of autoignition, however, is not evident and is matter for further work.

The parabolic CMC (CMCI and CMCII) equations have been discretized using the Method of Lines in a system of ODEs that has been implicitly integrated by the package VODPK [37]. A finite difference grid of 101 nodes clustered around $\xi_{ST} = 0.065$ have been used in η-space. The space-marching step was defined by the same stiff solver while the flow field were updated in intervals corresponding to the size of the fine CFD mesh. All thermodynamic properties including the Jacobian and the Hessian of the reaction rate in the Taylor expansion and the $P(T|\eta)$ in the Joint-PDF method have been calculated implicitly. $P(T|\eta)$ is evaluated at every η on a 51 node adaptive grid, which is a function of $\widehat{Q}_T$ and $\widehat{G}_{TT}$ to resolve the β-function shapes from the Gaussian to the J-shape. A δ-function is used instead of the β-function at low conditional temperature variance for conditions $\widehat{G}_{TT} < 1 \times 10^{-8}$. Equation (2), with the closure considered, requires the initial covariance to be initialized with a very small but finite value to start the second-moment calculation. $G_{ij} = 1 \times 10^{-50}$ has been enforced to all initial reactant covariances whose conditional mean mass fractions were finite.

3 Results and Discussion

3.1 Velocity and mixture fraction

Measurements of velocity and mixture fraction and its dissipation rate were available for similar configurations to the high temperature autoignition experiment. Initially the flow field has been validated against hot-wire measurement data for flow conditions of air injected into air at ambient temperature for the equal velocity case. Figure 2 shows the axial normalized mean (U/U_{BULK}) and root-mean square (r.m.s.) (u'/U) of velocity. Good agreement can be found in the inner region of the flow for both mean velocity and r.m.s.. The turbulence intensity increases in the region of high shear at the injector exit and the turbulence decays further downstream. An almost uniform profile for both velocity and turbulent intensity is recovered after $20d_{IN}$ in the inner region of the domain.

The mixing field has been validated against experimental measurements of acetone (C_3H_6O) Planar Laser Induced Fluorescence (PLIF) in a equal velocity coflow at ambient conditions. Figure 3 shows axial and radial plots for $\widetilde{\xi}$, $\widetilde{\xi''^2}$ and $\widetilde{\chi}$. The predictions are satisfactory although an under-prediction of the variance and of the scalar dissipation rate are evident for their initial rise at the injector exit. Validation of $\tilde{P}(\eta)$ and $\langle N|\eta \rangle$ have also been performed [23] and the β-PDF and the AMC model

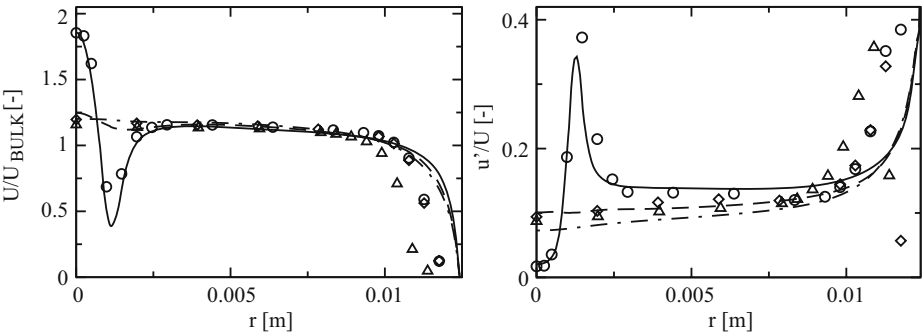

Fig. 2 Normalized axial velocity along the radial direction (*left*). Normalized r.m.s. of axial velocity along the radial direction at different axial locations (*right*). *Symbols*: experiment at 2 mm (*circle*), 22 mm (*diamond*), 42 mm (*triangle*). *Lines*: predictions at 2 mm (*solid*), 22 mm (*dashed*), 42 mm (*dashed-dotted*)

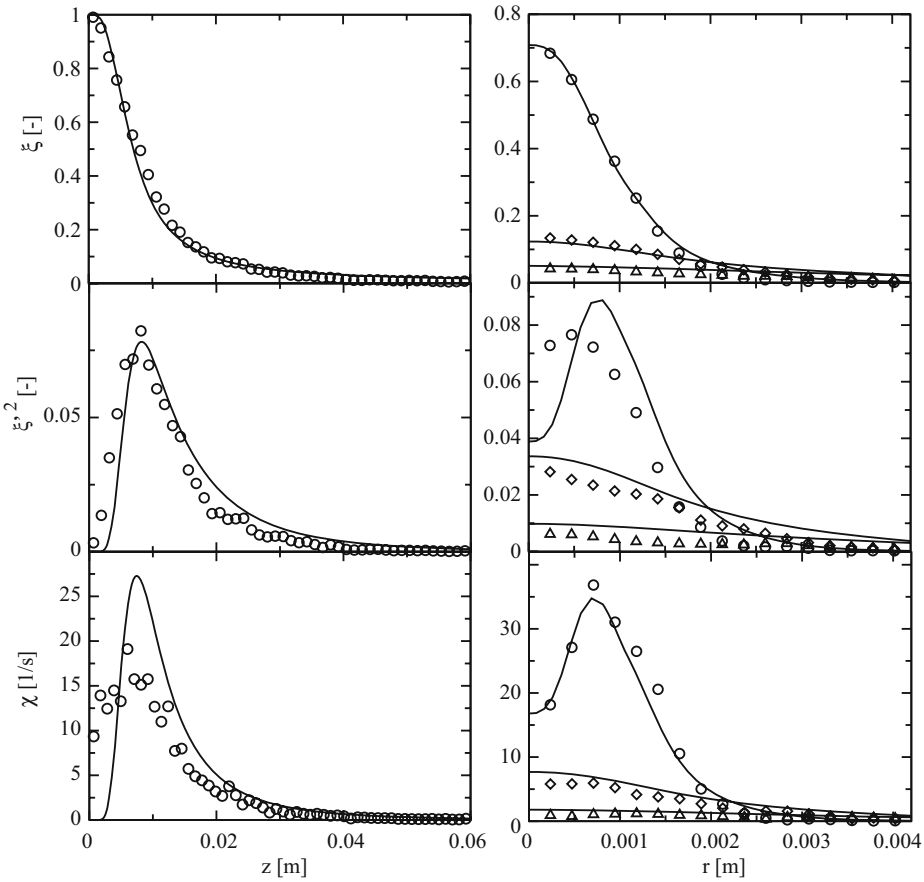

Fig. 3 $\widetilde{\xi}$, $\widetilde{\xi'^2}$, $\widetilde{\chi}$ along the axis (*left*) and the radial direction (*right*). *Symbols*: experiment at 5 mm (*circle*), 17 mm (*diamond*), 29 mm (*triangle*). *Lines*: predictions

were found acceptable overall. However, both models gave poor predictions close to the injector where a bimodal shape of the PDF was found in the experiment that it was not reproduced with a β-function, perhaps due to the under-prediction of the mixture fraction variance.

3.2 Description of the phenomena

Results obtained using a parabolic first-order closure have been presented previously [12]. Here, the main points are summarized to better understand the second-order formulation and its effect on autoignition. A global description of autoignition is given in Fig. 4 where plots of unconditional temperature ($\widetilde{T}$) and heat release rate ($\widetilde{W}_T$) are drawn along the axis. It can be seen that the autoignition location, which can be identified as a sudden increase in the average temperature, depends on T_{AIR}, as expected. After a small decrease of temperature at the injector exit due to endothermic reactions predicted by the mechanism at these conditions, the temperature starts rising monotonically with the distance from the injector. A qualitatively different behavior is observed at high and at low T_{AIR}, which is more evident from the plot of the heat release rate. At high T_{AIR}, $\widetilde{W}_T$ rises monotonically with the distance from the injector. As T_{AIR} decreases, $\widetilde{W}_T$ is reduced (the curves are less steep) and below a certain value $\widetilde{W}_T$ is stabilizing, or even decreasing, before autoignition occurs. In our previous work [12] this effect has been attributed to the effect of the mixture fraction statistics, which represents the transition between a non-premixed and a more homogeneous autoignition. The effect of the conditional scalar dissipation rate were also considered showing that increasing the conditional scalar dissipation rate, obtained by rising the bulk velocity keeping constant the velocity ratio of fuel and coflow, the autoignition location was non-linearly shifted downstream. This last effect was related to the time that fluid particles spend at high conditional scalar dissipation rate values close to the critical χ_{CR}. In the present coflow configuration the conditional scalar dissipation rate was decaying rapidly downstream the injector and the autoignition location was hence reasonably predicted by first-order closure.

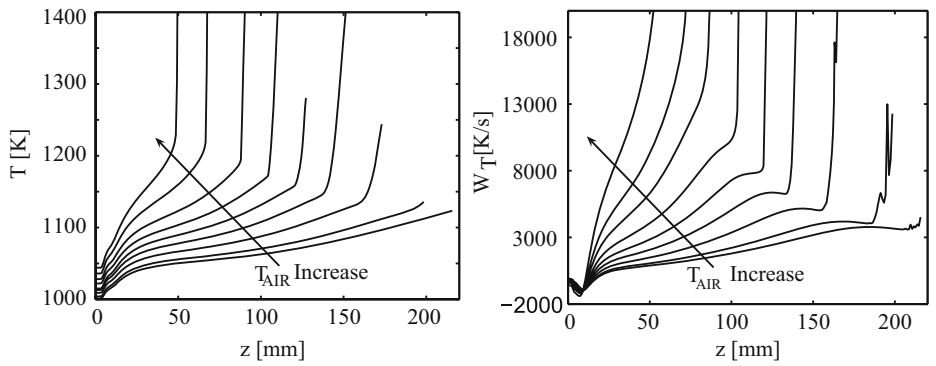

Fig. 4 Favre-mean temperature ($\widetilde{T}$) (*left*) and mean heat release rate ($\widetilde{W_T}$) (*right*) along the axis

3.3 CMC second-order closure

In the following, results for the three different second-order implementations are presented: (i) a second-order closure based on a Taylor expansion of the conditional reaction rate applied to all the reactive species in the mechanism, (ii) the same methodology as (i) but solving only for the temperature variance and (iii) a conditional joint PDF method restricted to the conditional PDF of temperature, $P(T|\eta)$.

3.3.1 Taylor expansion method—full second-order closure

Results in terms of autoignition length (L_{IGN}) are shown in Fig. 5 as function of the air temperature T_{AIR}. The calculated L_{IGN} using first and second-order closure are comparable and close to the experimental measurements. The differences between the ignition length predicted are expressed in term of the error parameter $\varepsilon = (L_{CMCI} - L_{CMCII})/L_{CMCI}$. Results are reported for method (i) as function of T_{AIR} and extended for the experimental point at $T_{AIR} = 1135$ K for methods (ii) and (iii). Sensitivity of the predictions to the term T_4, therefore to the scalar dissipation rate conditional fluctuations in (2) is presented. ε spans a small interval from very small negative values to less than 2%. Even though the overall predictions do not change substantially, the use of second-order closure gives better insight into the mechanism leading to autoignition.

The second-order CMC produces slightly earlier autoignition ($L_{CMCII} < L_{CMCI}$), consistent with [10]. ε increases at first as T_{AIR} increases to stabilize or even decay slightly at high temperature. This trend can be explained as the competition between two opposite effects: an increase in T_{AIR} moves the autoignition location upstream, hence in regions of higher conditional scalar dissipation rate and of higher scalar dissipation rate fluctuations, which would yield earlier autoignition predictions of second-order closure compared to the first-order ones. At the same time an increase in T_{AIR} results in an increase of χ_{CR} and a reduced time (or length) that the fluid spends above the critical conditions, resulting in a small difference between first and second-order predictions.

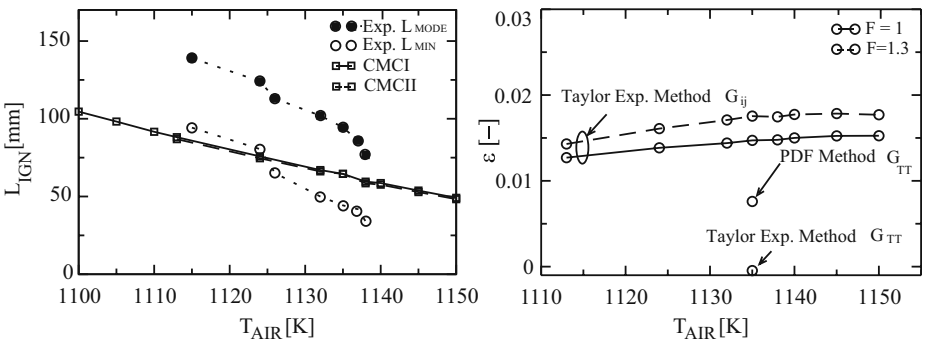

Fig. 5 Comparison of autoignition length from experiment and predictions (CMCI, CMCII) (*left*). The two experimental curves denote L_{MIN} (the shortest length) and L_{MODE}. *Right*: the relative difference in the predictions between first and second-order CMC

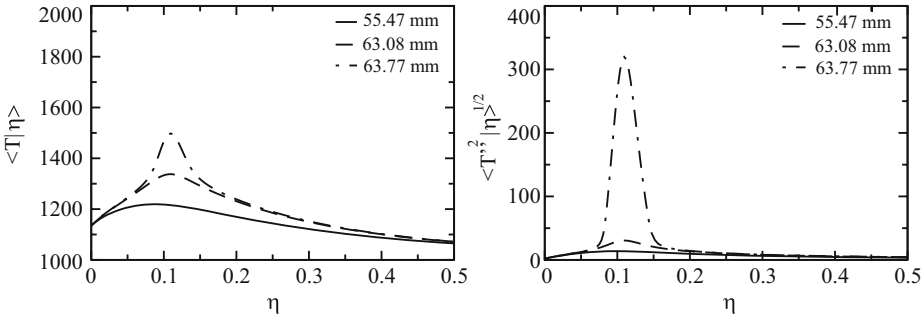

Fig. 6 Evolution of $\langle T|\eta\rangle$ (*left*) and $\langle T''^2|\eta\rangle^{1/2}$ (*right*) at 55.47 mm, 63.08 mm, 63.60 mm from the injector. Simulation conditions: $T_{AIR} = 1135K$, $T_{FU} = 1035$, $F = 1$

The importance of the conditional scalar dissipation rate fluctuations has been assessed by a sensitivity analysis on the constant F appearing in the model for the term T_4 (13). Increasing its value from 1 to 1.3 results in earlier predicted autoignition, consistent with the findings of [10]. We conclude therefore that second-order closure will be very important for conditions where the mean conditional scalar dissipation is high, approaching the critical value, *and* the conditional fluctuations are also large. Despite the fact that in the experiment studied here a delaying effect of autoignition due to high scalar dissipation was observed, the region of high scalar dissipation was not long enough to make the second-order effects result in a large difference in the prediction of the autoignition location.

Figure 6 shows the evolution of the conditional temperature and its root mean square (r.m.s) at condition $T_{AIR} = 1135K$ and $T_{FU} = 1035K$ for three locations close to autoignition. The conditional temperature and its fluctuations peak at ξ_{MR}, as expected. Autoignition is characterized by a sudden rise in conditional temperature fluctuations, which attain a segregation coefficient $\widehat{S}_T = \frac{\widehat{G}}{\widehat{Q}_T(1-\widehat{Q}_T)} \approx 0.85$, indicating an approximately bimodal behavior. Figure 7 shows the corresponding evolution of the conditional heat release rate as calculated from (8). Far from the inlet, where the reaction involves endothermic reactions, $\langle W_T^I|\eta\rangle$ is positive and increases

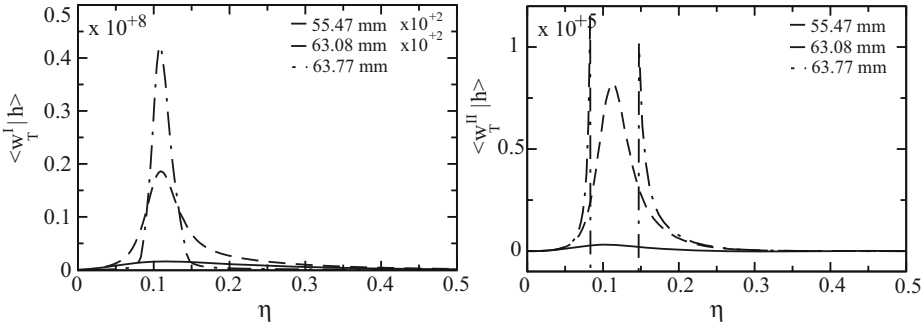

Fig. 7 Evolution of the conditional reaction rate first-order term (*left*), second-order term (*right*). Simulation conditions as in Fig. 6

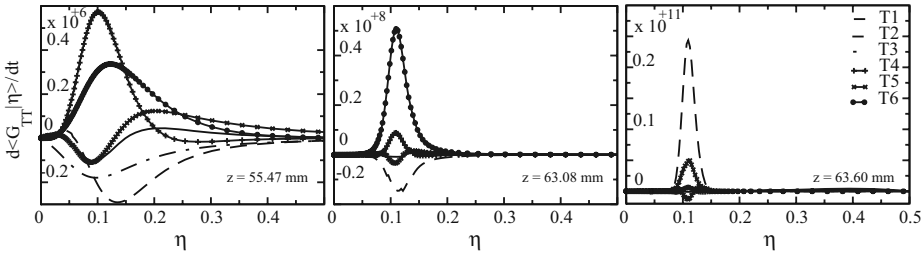

Fig. 8 Balance of terms in the G_{TT} transport equation at 55.47 mm (*left*), 63.08 mm (*center*), 63.60 mm (*right*) from the injector. Simulation conditions as in Fig. 6

monotonically. $\langle W_T^{II}|\eta\rangle$ behaves differently: it enhances autoignition during the pre-ignition phase but at autoignition changes its sign at ξ_{MR}, while showing a double front in the vicinity of ξ_{MR}. This can be explained since at autoignition $\langle W_T^{I}|\eta\rangle$ is close to a maximum, therefore any perturbations as due to a second-order correction yields a negative contribution.

Calculations using the Taylor expansion method couldn't proceed after autoignition. The second-order truncation of the Taylor expansion of the reaction rate becomes inappropriate during the thermal 'run-away' at autoignition when, as saw from Fig. 11, the conditional fluctuations become very large, closure higher than second-order might be needed.

Figure 8 shows the balance of terms in the variance equation for temperature at the same location as Fig. 6. In the pre-ignition phase, T_4, which involves the conditional scalar dissipation rate fluctuations, is the driving term (consistent with [10]), and is mainly balanced by the reaction rate term T_2. Approaching autoignition the gradient term T_6 becomes important together with T_4 still balanced by T_2.

3.3.2 Taylor expansion method—conditional temperature variance

In the aim of simplifying the system of equations to solve, a closure based on the temperature variance has been attempted. Under this assumption the reaction rate Hessian reduces to its second derivative with respect to temperature. Autoignition lengths for conditions $T_{AIR} = 1135K$ and $T_{FU} = 1035K$, and using $F = 1$, are shown in Fig. 5. The error parameter ε becomes negative, indicating an increase in the autoignition length with respect to a first-order closure. The evolution of the conditional temperature and its fluctuations is shown in Fig. 9 for different locations before, during and after the autoignition event. The selected locations are, when possible, as in Fig. 6 so as to compare results directly with the different methodologies. The use of the additional transport equation for the conditional temperature variance was solved without numerical instabilities after ignition allowing the modelling of the autoignition and the hot kernel propagation. The conditional temperature fluctuations evolve in similar manner as in Fig. 6. It is noticeable how after the first peak at autoignition, two peaks corresponding to two flame fronts arise.

Figure 10 shows the evolution of $\langle W_T^{I}|\eta\rangle$ and $\langle W_T^{II}|\eta\rangle$. The first-order term in the reaction rate shows the development of a triple flame after ignition. The flame fronts visible in $\langle W_T^{I}|\eta\rangle$ are much narrower than the ones inferred from the fluctuating temperature that involve broader regions. The evolution of $\langle W_T^{II}|\eta\rangle$ gives an ex-

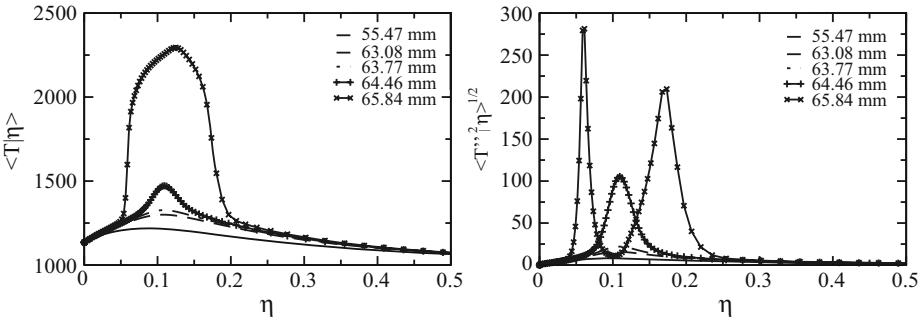

Fig. 9 Evolution of $\langle T|\eta\rangle$ (*left*) and $\langle T''^2|\eta\rangle^{1/2}$ (*right*) at the indicated distance from the injector. CMCII predictions using a Taylor expansion method solving for only the G_{TT} transport equation. Simulation conditions: $T_{AIR} = 1135K$, $T_{FU} = 1035$, $F = 1$.

planation for the increase in autoignition length using a second-order formulation. During the pre-ignition reaction leading to autoignition, the chemistry does not behave as an exponential function with temperature (see also Fig. 4). Mathematically, temperature is still a monotonic function with positive first derivative since a positive perturbation produces a positive variation of the reaction rate, but its second derivative, represented by the Hessian of the temperature production rate with respect to temperature is negative. This explains the initial negative contribution of the second-order correction that yields to a retardation of autoignition. After ignition $\langle W_T^{II}|\eta\rangle$ acts in two opposite ways. It reduces the reaction rate in the inner regions of the flame fronts while enhances the propagation in the flame adjacent area.

Reducing a second order closure formulation using a Taylor expansion method to the integration of the temperature variance equation, may yield inaccurate prediction of autoignition problems. Depending on the chemistry a more suitable scalar or composition of scalars may be chosen. However, this simplified methodology offers a stable and computationally efficient way to introduce the effects of conditional fluctuations in CMC to evaluate autoignition and flame propagation.

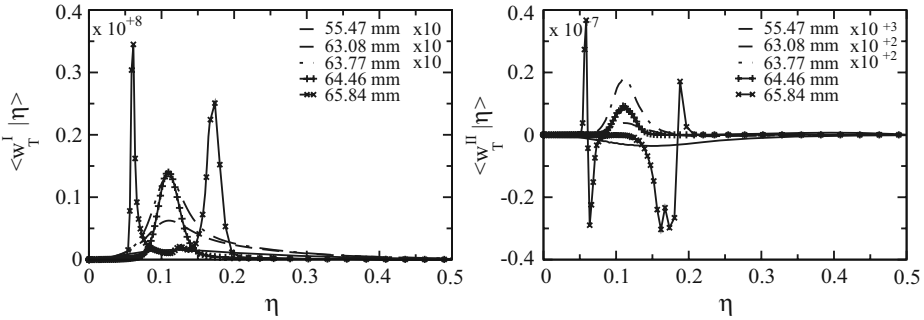

Fig. 10 Evolution of the conditional reaction rate first-order term (W_T^I) (*left*), second-order term (W_T^{II}) (*right*). Simulation conditions as in Fig. 9

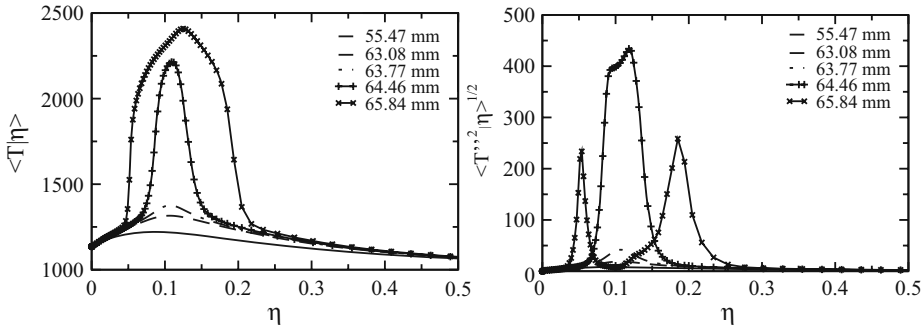

Fig. 11 Evolution of $\langle T|\eta\rangle$ (*left*) and $\langle T''^2|\eta\rangle^{1/2}$ (*right*) at the indicated distance from the injector. CMCII predictions using the conditional joint-PDF method solving for only the G_{TT} transport equation. Simulation conditions: $T_{AIR} = 1135K$, $T_{FU} = 1035$, $F = 1$

3.3.3 PDF method—conditional temperature variance

Alternative to the Taylor expansion, the joint-PDF method offers the possibility to close the reaction rate without assumption on the magnitude of the conditional scalar fluctuations. As for the previous test cases, the autoignition lengths are shown in Fig. 5 for $F = 1$. The conditional temperature and its fluctuations are presented in Fig. 11 for the same locations considered in the Taylor expansion method. Autoignition occurs at earlier times compared to Fig. 9 so that the plots are at a time closer to ignition. Figure 12 show the evolution of the conditional temperature production rate as calculated by (10). The different phases of ignition, double flame propagating into a triple flame are evident.

Figure 13 shows, at the same location as in Fig. 11, the evolution of $P(T|\eta)$. The temperature is bounded between the frozen and equilibrium limits. Starting from a narrow $P(T|\eta)$ due to the low variance, as the reactions proceed, in the region of ξ_{MR} the $P(T|\eta)$ becomes broader leading to autoignition, represented by a J-shape. The subsequent flame propagation is clearly visible from the bimodal shape of the PDF at the η corresponding to the flame fronts. The shapes of $P(T|\eta)$ are consistent with the one reported in [1].

The conditional joint-PDF method, even with the simplified approach of solving only for the temperature variance, results in good prediction of the autoignition delay

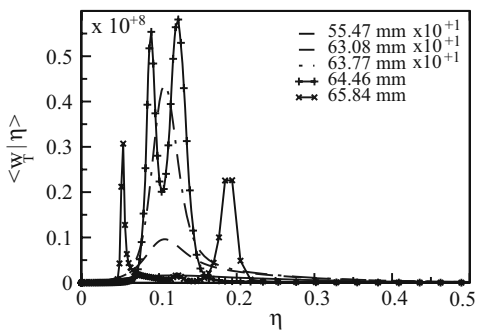

Fig. 12 Evolution of the conditional reaction rate for conditions as in Fig. 11

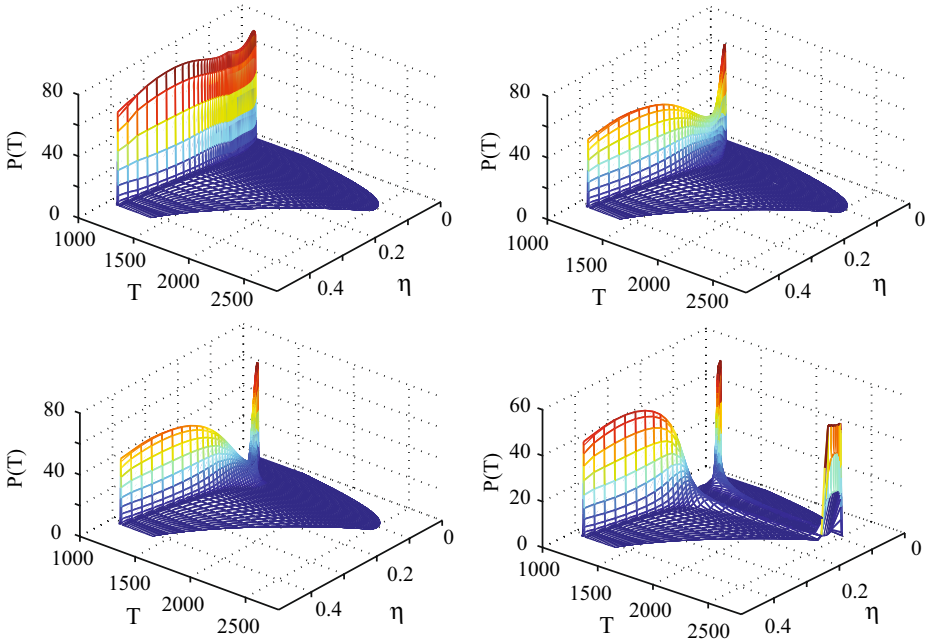

Fig. 13 Evolution of $P(T|\eta)$ at 55.47 mm (*top left*), 63.08 mm (*top right*), 63.77 mm (*bottom left*), 64.46 mm (*bottom right*), from the injector. Conditions as in Fig. 11

with the additional advantage that no restriction on the magnitude of the conditional fluctuations has to be considered and therefore it is valid for both autoignition and flame propagation. Its main limitation is the mathematical description for the conditional PDF and its bounds. At autoignition, from laminar autoignition theory [31], the lower branch of the S-shape does not correspond to the frozen mixing of the reactants but to somehow higher temperature. This implies that at autoignition in turbulent cases the lower bound should evolve during the calculation. A possible lower limit could be the conditional temperature calculated with a conditional scalar dissipation rate higher than the critical value.

4 Conclusions

The conditional moment closure model has been applied to model autoignition of an n-heptane plume in a turbulent heated air coflow. A parabolic, cross-stream integrated formulation has been implemented. The conditional reaction rate has been closed using first and second-order closure. Three methodologies have been implemented for the second-order closure, a Taylor expansion method solving for the full matrix of variances and covariances of the species in the chemical mechanism, a simplified Taylor expansion method using only the temperature variance and a conditional joint-PDF method in which only the temperature conditional variance has been used to evaluate the conditional reaction rate, presuming the conditional temperature PDF to be a β-function.

The second order-closure, using a Taylor expansion method applied to all species, predicts shorter autoignition lengths than first-order closure consistent with DNS results and in good agreement with experiment. The conditional scalar fluctuations enhance autoignition. The driving term in the conditional covariance equation, during an autoignition calculation, is the one dependent on the conditional scalar dissipation rate fluctuations. Similar results have been found with the other second-order closure methods tested here. In the present case first and second-order closure had small differences in the predictions. The reason is attributed to the rapid decay of the conditional scalar dissipation rate below its critical value. First-order closure appears, therefore, to be adequate at these conditions.

The Taylor expansion method can predict autoignition. However, it is inappropriate to predict the subsequent kernel development. The conditional temperature PDF method resulted in numerically stable predictions and can be applied to autoignition as well as flame development with careful definition of the PDF bounds.

References

1. Mastorakos, E., Baritaud, T.A., Poinsot, T.J.: Numerical simulations of autoignition in turbulent mixing flows. Combust. Flame **109**, 198–223 (1997)
2. Im, H.G., Chen, J.H., Law, C.K.: Ignition of hydrogen-air mixing layer in turbulent flows. Proc. Combust. Inst. **27**, 1047–1056 (1998)
3. Sreedhara S., Lakshmisha, K.N.: Autoignition in a non-premixed medium: DNS studies on the effects of three-dimensional turbulence. Proc. Combust. Inst. **29**, 2051–2059 (2002)
4. Echekki, T., Chen, J.H.: Direct numerical simulation of autoignition in non-homogeneous hydrogen-air mixtures. Combust. Flame **134**, 169–191 (2003)
5. Wang, Y., Rutland, C.J.: Direct numerical simulation of ignition in turbulent n-heptane liquid-fuel spray jets. Combust. Flame **149**(4), 353–365 (2007)
6. Mastorakos, E., Pirez Da Cruz, A., Baritaud, T.A., Poinsot, T.J.: A model for the effects of mixing on the autoignition of turbulent flows. Combust. Sci. Technol. **125**, 243–282 (1997)
7. Liñan, A., Crespo A.: An asymptotic analysis of unsteady diffusion flames for large activation energies. Combust. Sci. Technol. **14**(1), 95–117 (1976)
8. Thevenin, D., Candel, S.: Ignition dinamics of a diffusion flame rolled up in a vortex. Phys. Fluids **4**, 434 (1995)
9. Klimenko, A.Y., Bilger, R.W.: Conditional moment closure for turbulent combustion. Prog. Energy Combust. Sci. **25**, 595–687 (1999)
10. Mastorakos, E., Bilger, R.W.: Second-order conditional moment closure for the autoignition of turbulent flows. Phys. Fluids **31**(6), 1246–1248 (1998)
11. Sreedhara, S., Lakshmisha, K.N.: Assessment of conditional moment closure models of turbulent autoignition using DNS data. Proc. Combust. Inst. **29**, 2069–2077 (2002)
12. Markides, C.N., De Paola, G., Mastorakos. E.: Measurements and simulations of mixing and autoignition of an n-heptane plume in a turbulent flow of heated air. Exp. Therm. Fluid Sci. **31**, 393–401 (2007)
13. Cha, C.M., Pitsch, H.: Higher-order conditional moment closure modelling of local extinction and reignition in turbulent combustion. Combust. Theory Model. **6**, 425–437 (2002)
14. Sreedhara, S., Huh, K.Y.: Modeling of turbulent, two-dimensional nonpremixed CH4/H2 flame over a bluffbody using first- and second-order elliptic conditional moment closures. Combust. Flame. **143**, 119–134 (2005)
15. Fairweather, M., Woolley, R.M.: First- and second-order elliptic conditional moment closure calculations of piloted methane diffusion flames. Combust. Flame **150**(1–2), 92–107 (2007)
16. Markides, C.N., Mastorakos, E.: An experimental study of hydrogen autoigniton in a turbulent co-flow of heated air. Proc. Combust. Inst. **30**, 883–891 (2005)
17. Markides, C.N., Mastorakos, E.: Measurements of scalar dissipation in a turbulent plume with planar laser-induced fluorescence of acetone. Chem. Eng. Sci. **61**(9), 2835–2842 (2006)
18. Galpin, J., Angelberger, C., Naudin, A., L. Vervisch, L.: Large-eddy simulation of H2-air autoignition using tabulated detailed chemistry. J. Turbul. **9**, 13 (2008)

19. Jones, W.P., Navarro-Martinez, S.: Study of hydrogen auto-ignition in a turbulent air co-flow using a Large Eddy Simulation approach. Comput. Fluids **37**(7), 802–808 (2008)
20. FLUENT (2003) FLUENT V6. http://www.fluent.com. Accessed 2003
21. Kim, I.S., Mastorakos, E.: Simulations of turbulent non-premixed counter-flow flames with first-order conditional moment closure. Flow Turbul. Combust. **76**, 133–162 (2006)
22. Klimenko, A.Y.: Note on the conditional moment closure in turbulent shear flows. Phys. Fluids **7**(2), 446–448 (1995)
23. De Paola, G.: Conditional moment closure for autoignition in turbulent flows. PhD Thesis, University of Cambridge (2007)
24. Markides, C.N., Mastorakos, E.: Measurements of the statistical distribution of the scalar dissipation rate in turbulent axisymmetric plumes. Flow Turbul. Combust. **81**, 221–234 (2008)
25. Devaud, C.B., Bray, K.N.C.: Assessment of the applicability of conditional moment closure to a lifted turbulent flame. Phys. Fluids **16**(6), 2004–2011 (2004)
26. Bikas, G.: Kinetic mechanisms for hydrocarbon ignition. PhD Thesis, University of Aachen (2001)
27. Hewson, J.C.: Pollutant emission from non premixes hydrocarbon flames. PhD Thesis, University of California, San Diego (1997)
28. Wright, Y.M., De Paola, G., Boulouchos, K., Mastorakos, E.: Simulation of spray autoignition and flame establishment with two-dimensional CMC. Combust. Flame **143**, 402–419 (2005)
29. Kim, S.H., Huh, K.Y., Bilger, R.W.: Second-Order conditional moment closure modeling of local extinction and reignition in turbulent non-premixed hydrocarbon flames. Proc. Combust. Inst. **29**, 2131–2137 (2002)
30. Sreedhara, S., Huh, K.Y.: Assessment of closure schemes in second-order conditional moment closure against DNS with extinction and ignition. Combust. Flame **143**, 386–401 (2005)
31. Liñan, A.: The asymptotic structure of counterflow diffusion flames for large activation energies. Acta Astronaut. **1**, 1007 (1974)
32. Kronenburg, A., Kostka, M.: Modeling extinction and reignition in turbulent flames. Combust. Flame **143**, 342–356 (2005)
33. Swaminathan, N., Bilger, R.W.: Study of the conditional covariance and variance equations for second order conditional moment closure. Phys. Fluids **11**(9), 2679–2695 (1999)
34. Li, J.D., Bilger, R.W.: Measurement and prediction of the conditional variance in a turbulent reactive-scalar mixing layer. Phys. Fluids A **5**(12), 3255–3264 (1993)
35. Cao, S., Echekki, T.: Autoignition in nonhomogeneous mixtures: conditional statistics and implications for modeling. Combust. Flame **151**(1–2), 120–141 (2007)
36. Kim, S.H.: On the conditional variance and covariance equations for second-order conditional moment closure. Phys. Fluids **14**(6), 2011–2014 (2002)
37. Brown, P.N., Byrne, G.D., Hindmarsh, A.C.: VODE, a variable-coefficient ODE solver. SIAM J. Sci. Stat. Comput. **10**, 1038–1051 (1989)